Appl. Phys. A (2005)
DOI: 10.1007/s00339-005-3350-x

Applied Physics A
Materials Science & Processing

T. IRAWAN[1]
D. BOECKER[1]
F. GHALEH[1]
C. YIN[2]
B. VON ISSENDORFF[2]
H. HÖVEL[1,✉]

Metal clusters on rare gas layers – growth and spectroscopy

[1] Universität Dortmund, Experimentelle Physik I, 44221 Dortmund, Germany
[2] Universität Freiburg, Fakultät für Physik, 79104 Freiburg, Germany

Received: 6 February 2005/Accepted: 6 July 2005

ABSTRACT Gold and lead clusters were grown by the evaporation of metal atoms on rare gas layers on Au(111) and Pb(111). The growth was investigated with scanning tunneling microscopy (STM) and ultraviolet photoelectron spectroscopy (UPS). We studied the electronic coupling to the surface and charging effects in the photoemission process. For a rare gas film thickness of 60 ML we observed an electronic decoupling: the cluster spectra are no longer referenced to the Fermi edge, but to the vacuum energy of the substrate. For Pb clusters on a Au(111) substrate this leads to the remarkable result of a cluster-photoelectron signal above the Fermi energy defined by the ground level of the sample holder.

PACS 33.60.Cv; 36.40.Mr; 68.37.Ef; 61.46.+w; 73.22.-f

1 Introduction

Rare gas layers were used in several experiments to reduce the interaction between metal islands or clusters grown or deposited on surfaces. We mention only two typical examples. The deposition of Pt atoms and small Pt clusters into a thin rare gas layer on a graphite surface was used to study the influence of the cluster-surface interaction [1]. The rare gas strongly reduced the surface diffusion and specific shifts induced by an interaction of the clusters with defects such as step edges could be identified. In [2] Ag atoms were evaporated on a Xe layer on GaAs. The formation of Ag clusters and the subsequent immersion of the clusters into the Xe film were studied with X-ray photoelectron spectroscopy. Later this method was refined and called Buffer Layer Assisted Growth (BLAG), see [3]. We used this method to produce gold or lead clusters on xenon or argon films on one of the following surfaces: a single crystal of Pb(111) or Au(111) or a 100 nm Au(111) film on mica.

These experiments are motivated by future experiments when we will compare the results of free clusters in vacuum with the same clusters on surfaces. A magnetron sputter gas aggregation cluster source [4] with a semi-continuous time-of-flight mass selector [5] will be used to deposit mass-selected clusters onto a substrate. In this context rare gas films will be used for two different reasons. For the deposition process they will help to realize soft landing conditions for the size selected clusters. In addition the rare gas film can be used to decouple the electronic system of the clusters from the substrate surface. Using varying coupling to the surface, we will investigate the electronic structure of the metal clusters with UPS and, if possible, also with STS at low temperatures.

Therefore we investigated in this study several cluster/rare gas/substrate systems, produced by BLAG. We grew on a cold sample rare gas layers with a thickness of 10–120 ML and evaporated a specific amount of metal which forms clusters on the rare gas surface. The results show that we decoupled the clusters electronically from the substrate by a rare gas film of 60 monolayers (ML) thickness. This leads to a change of the reference energy. The cluster spectra are no longer referenced to the Fermi edge but to the vacuum energy. This is similar for free clusters in a cluster beam. However, here the vacuum energy is not a constant parameter of the apparatus but determined by the material of the substrate. In this sense one can call the clusters decoupled by a rare gas layer "free clusters on substrate".

2 Experimental

For the investigation of cluster/rare gas/substrate systems, as performed here, an exact measurement of the thickness of the rare gas layer is essential. We used an in-situ control of the film thickness during monolayer by monolayer adsorption of the rare gas films by observing the $5p_{1/2}$ and $5p_{3/2}$ signal in situ with UPS, while xenon was introduced in the preparation chamber. One can observe the polarization induced shift between the first and second ML [6] and the quantum well states for larger film thicknesses [7]. The controlled rare gas adsorption process is shown in Fig. 1, where the UPS spectra are displayed in a color coded plot versus the adsorption time. We established a xenon pressure $p_{\mathrm{Xe}} = 1.5 \times 10^{-7}$ mbar for a time $t = 2450$ s. The sample temperature during the adsorption was $T_{\mathrm{sample}} \approx 30$ K. At this temperature the diffusion of xenon on the sample surface is fast enough to allow a layer by layer growth, but the temperature is low enough for the adsorption of multilayers of xenon. In case of too low sample temperatures during xenon adsorption we were not able to observe the characteristic UPS spectra for each monolayer, because a rough film was

✉ Fax: +49-231-755-3657, E-mail: hoevel@physik.uni-dortmund.de

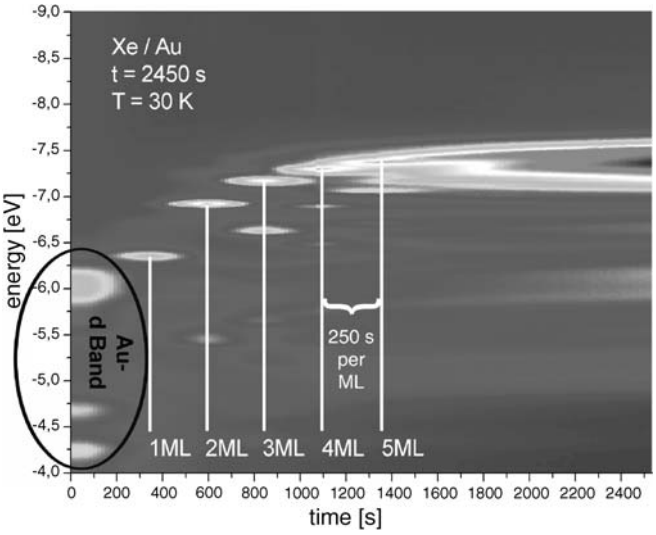

FIGURE 1 Controlled xenon adsorption on Au(111) by using a color coded display of the UPS data. The Au-d band signal disappeared, while Xe was introduced in the preparation chamber with a pressure $p_{\mathrm{Xe}} = 1.5 \times 10^{-7}$ mbar at a temperature $T = 30$ K. The exact xenon layer thickness was obtained from the characteristic UPS spectra for the $5p_{1/2}$ signal of Xe for one to five ML xenon coverage and an extrapolation of the adsorption time for larger film thicknesses. Also the $5p_{3/2}$ signal is visible, e.g., at about -5.5 eV for 2 ML and 3 ML

grown. At $t = 0$ s the Au d-bands are visible. When xenon is introduced in the preparation chamber after $t = 90$ s the Au d-bands vanish and the characteristic xenon $5p_{1/2}$ peak of the first monolayer increases and finally decreases again. In equidistant time intervals $5p_{1/2}$ peaks of the second, third, fourth, and fifth monolayer increase and decrease in the same way. For film thicknesses larger than about 5 ML the adsorption time can be extrapolated. In this way we are able to produce well-defined xenon layers with known thicknesses by counting the monolayers of xenon. The next step in the preparation process is to produce the metal clusters on the rare gas film.

Therefore the metal, in our case lead or gold, is deposited onto the sample. The amount of evaporated gold is controlled by an integrated flux monitor and a calibration measurement. For details of the calibration see [8].

For the interpretation of the observed effects reported in the next section the work function is of particular importance. We always measure the work function of the samples at several steps in an experimental run. The work functions are given by

$$\Phi_{\mathrm{S}} = h\nu - \Delta E_{\mathrm{spectra}}\,, \tag{1}$$

where $h\nu = 21.2$ eV is the photon energy and $\Delta E_{\mathrm{spectra}}$ is the total width of the photoelectron spectra. To obtain $\Delta E_{\mathrm{spectra}}$ we apply a bias voltage of $U_{\mathrm{bias}} = 5.00$ V to the sample and determine the position of the Fermi energy and of the lower so called cut off energy, which is given by the onset of the secondary electron peak [9] (cf. Fig. 8).

3 Results and discussion

We investigated several combinations of Au and Pb clusters, Ar and Xe films, and Au(111) and Pb(111) substrates. We differentiate between *symmetric systems* such as Pb clusters on rare gas on a Pb(111) substrate and *asymmetric systems* such as Au clusters on rare gas on a Pb(111) substrate. The nomenclature is as follows: cluster/rare gas/substrate; e.g., Pb/Xe/Pb or Au/Xe/Pb, respectively.

To decouple the clusters from the surface, we prepared different thicknesses of the rare gas layer. We started with Au clusters on 10 ML Xe on Pb(111). In the UPS spectra the Fermi-level onset of the gold clusters had the same energetic position as the pristine Pb(111) substrate measured before adsorption. We then transferred the cold sample into the analysis chamber and imaged the clusters with the STM at a temperature of 5 K. STM images of the gold clusters before and after desorption of the xenon are shown in Fig. 2. The amount of gold is described as an effective film thickness, in this case 3.6 ML Au. The xenon was desorbed by increasing the sample temperature to 100 K for some minutes.

The cluster density before the desorption of the Xe film was determined by averaging four different 50×50 nm^2 sized STM images. Stable imaging of larger sample areas was not possible. One obtains 206 ± 14 clusters per 10^4 nm^2. After the desorption of the xenon we were able to image four 100×100 nm^2 sized areas and the cluster density is 204 ± 7 clusters per 10^4 nm^2. After Xe desorption the clusters form larger aggregates, but the individual clusters still can be identified. In addition to the statistical errors given above, systematic errors have to be considered for STM imaging, e.g., the changing of the tip shape and the resulting distortion of the cluster shape by tip-cluster convolution [10]. We estimate that this will lead to systematic errors at least of 10% for the cluster density. In [11] no significant coalescence during desorption was observed for a rare gas film thickness below 10 ML. Imaging clusters with a 10 ML xenon layer before desorption indicates

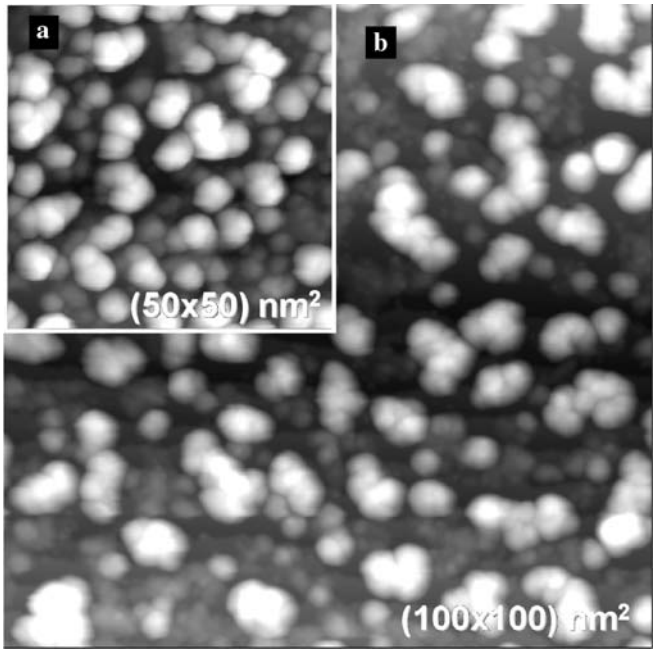

FIGURE 2 STM images ($T = 5$ K) for 3.6 ML Au on 10 ML Xe/Pb(111) (**a**) STM image before Xe desorption, ≈ 206 clusters per 10^4 nm^2 ($U_{\mathrm{T}} = 1.3$ V, $I_{\mathrm{T}} = 10$ pA) (**b**) STM image after Xe desorption, ≈ 204 clusters per 10^4 nm^2 ($U_{\mathrm{T}} = 1.5$ V, $I_{\mathrm{T}} = 20$ pA)

that the clusters are not completely decoupled, but have some contact to the substrate, which would be consistent with the position of the cluster Fermi edge in the UPS spectra. The thickness of a 10 ML xenon film is 2.48 nm and consequently in the same order of magnitude as the average height of the gold clusters, which is ≈ 2 nm as measured after the Xe film desorption. We assume that the clusters are partly or totally immersed in the xenon film and establish in this way the tunneling contact for imaging the clusters with STM.

For this reason we used in all following experiments 60 ML of xenon to be sure that even immersed clusters still have no contact to the substrate. To check that no simple static charging of the xenon film is present, we investigated a sample with a xenon layer up to 120 ML thickness and did not see any change in the xenon spectra. For static charging one expects a clearly visible shift of the xenon $5p_{1/2}$ peak to lower energies. Figure 3 summarizes the results for the asymmetric system Au clusters on 60 ML Xe on Pb(111). We display from bottom to top UPS spectra at important steps in the preparation of the sample system. In the spectra of the pristine Pb(111) surface, the sharp Fermi edge of the lead substrate is located at the reference Fermi edge, which is set to 0 eV.

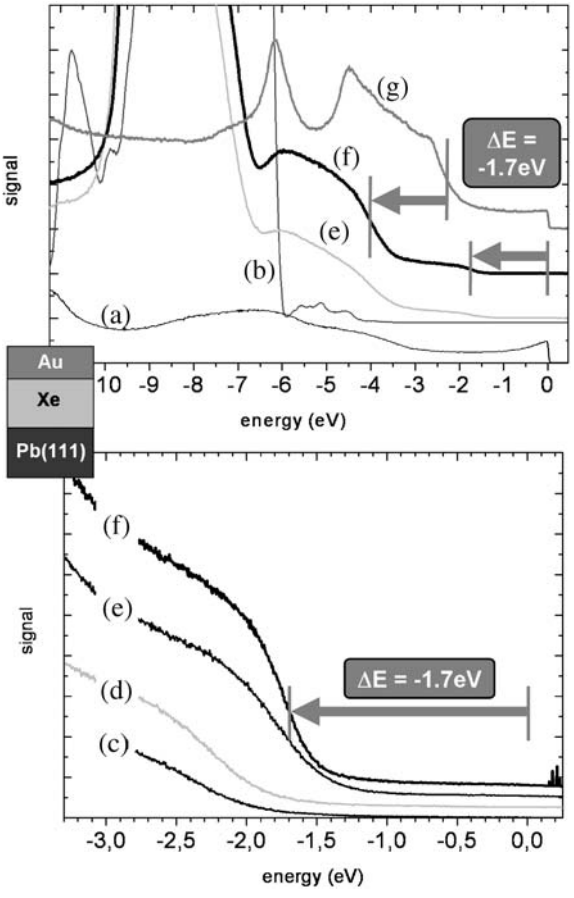

FIGURE 3 (*top*) UPS spectra: (a) pristine Pb(111) surface, (b) after xenon adsorption (60 ML), (e) after evaporation of 1.8 ML Au on 60 ML xenon/Pb(111), (f) with a total amount of 3 ML Au on 60 ML xenon/Pb(111) and (g) after xenon desorption. (*bottom*) Fermi edge spectra for a different amount of gold. (c) 0.6 ML, (d) 1.2 ML, (e) 1.8 ML and (f) 3.0 ML Au on 60 ML xenon/Pb(111). Because of $\Phi_{Pb} < \Phi_{Au}$ the Fermi edge of the Au clusters is shifted to *lower* energy, compared to the Fermi energy (0 eV) of the substrate

After the adsorption of 60 ML xenon, the signal of the Fermi edge vanishes. Gold was evaporated onto the xenon covered surface in four steps and UPS spectra were taken after each evaporation step (two are shown in Fig. 3 top). One observes a Fermi edge growing stronger with an increasing amount of evaporated gold, which is shifted about -1.7 eV compared to the reference Fermi energy. The same shift occurs for the onset of the d-band (-2.4 eV $\rightarrow$ -4.1 eV). The bottom of Fig. 3 shows the Fermi edge region of the spectra after each evaporation step. The spectra with different coverage amounts were mainly used to confirm that the signal of the cluster features is increasing with coverage. We do not discuss the differences for the different coverage amounts, but always measure the shift for the largest coverage of about 3 ML. More quantitative studies for the cluster-size dependent shifts will be the topic of future studies with mass-selected clusters. The Fermi edge is pronounced in the spectra for 3 ML Au and a shift of -1.7 eV is clearly visible here. This is a surprisingly large shift. For cluster sizes of a few nanometers the deviations to the bulk material should be small. But we can explain it as displayed in Fig. 4, which shows a schematic diagram for the Fermi edge shifts in the UPS spectra in analogy to Photoemission of Adsorbed Xenon (PAX) [12, 13].

In principle, the work function Φ is highly sensitive to changes concerning the surface. So it may be size dependent for small clusters. For the large cluster sizes considered here we assume that Φ for the cluster material is approximately the same as for the corresponding bulk material. The left side shows the above mentioned sample system Au/Xe/Pb together with the Pb(111) substrate. The measured Fermi energies E_F of Pb(111) and Au(111) are equal to the reference Fermi energy of the apparatus. This is because all metal substrates are electrically connected to the apparatus body via the sample holder and therefore on earth potential, symbolized by the ground icon. The decoupled gold clusters on the

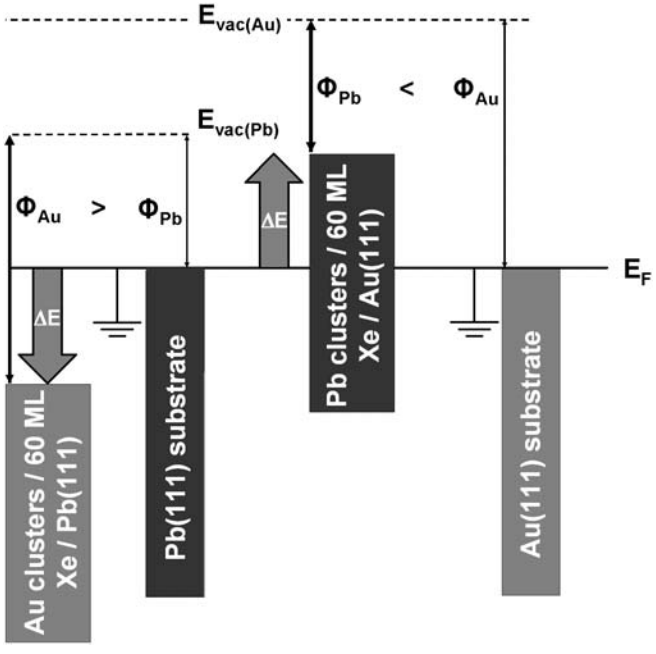

FIGURE 4 Schematic diagram for the Fermi edge shifts ΔE in our UPS spectra in analogy to Photoemission of Adsorbed Xenon (PAX), cf. [12]

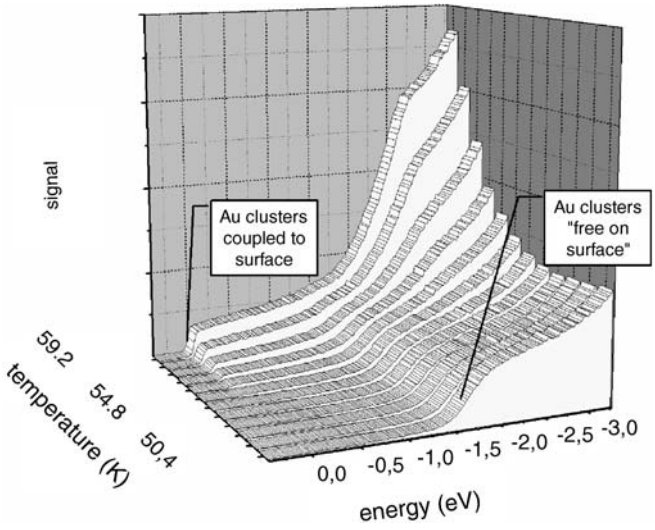

FIGURE 5 Change of the UPS spectra for Au Clusters on 60 ML Xe/Pb(111) during controlled heating of the sample from 50 K to 60 K with a rate of 0.2 K/min. One observes a constant decrease of the shifted Fermi edge of Au clusters on xenon until it vanishes completely, while the Fermi edge of the Pb substrate and of the clusters coupled to the substrate arise at the reference Fermi energy of 0 eV

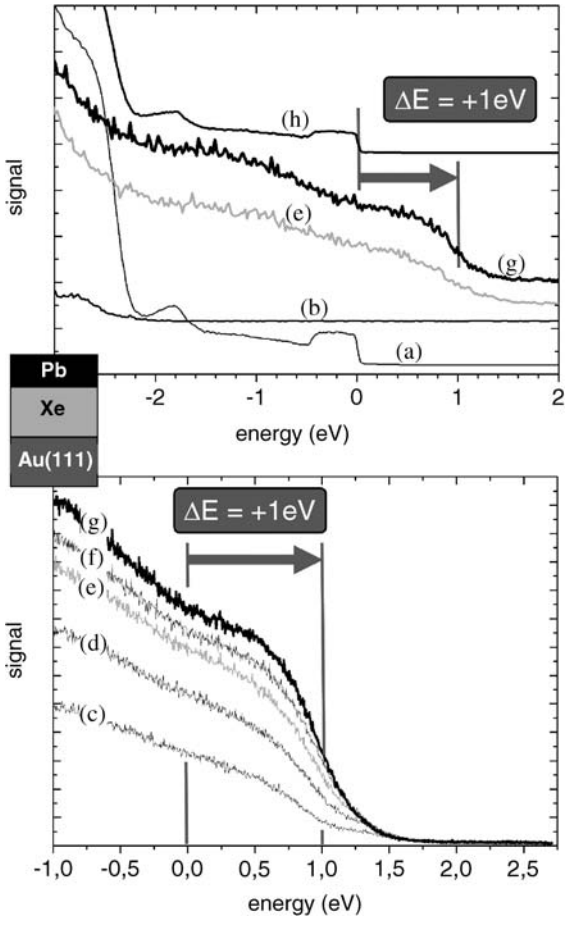

FIGURE 6 (*top*) UPS spectra: (a) pristine Au(111) surface, (b) after xenon adsorption (60 ML), (e) after evaporation of 1.5 ML Pb on 60 ML xenon/Au(111), (g) with a total amount of 2.5 ML Pb on 60 ML xenon/Au(111) and (h) after xenon desorption. The box-shaped structure from about -0.5 eV to 0 eV for samples (a) and (h) is due to the angle integrated signal of the Shockley surface state on Au(111). The fact that it is still visible for sample (h) after the Xe desorption shows that the sample stayed rather clean during all the preparation steps. (*bottom*) Fermi edge spectra for different amounts of lead: (c) 0.5 ML, (d) 1.0 ML, (e) 1.5 ML, (f) 2.0 ML and (g) 2.5 ML Pb on 60 ML xenon/Au(111). Because of $\Phi_{Au} > \Phi_{Pb}$ the Fermi edge of Pb clusters is shifted to *higher* energies, compared to the Fermi energy (0 eV) of the substrate

Au/Xe/Pb sample are no longer referenced to the Fermi edge but to the vacuum energy $E_{vac(Pb)}$ of the Pb(111) substrate. This is similar to the behavior of the Xenon $5p_{1/2}$ and $5p_{3/2}$ signals, which is the basis of PAX. In this way the existing work function difference $\Delta\Phi$ between Φ_{Au} and Φ_{Pb} leads to a shift ΔE of the cluster Fermi edge. The work function of lead is smaller than the work function of gold resulting in a shift of the gold-cluster Fermi edge to lower energies < 0 eV. We mention here that this change of the reference energy for decoupled clusters was also discussed in other studies [2, 14]. But in these experiments core level signals of the cluster material were measured that might be affected by additional shift mechanisms, as e.g., core level shifts due to the large number of surface atoms in clusters [15] or due to lattice strain [16]. In our experiments we observed further evidence for the decoupling of the clusters from the surface by measuring UPS during controlled sample heating. UPS spectra were taken continuously while heating the sample from 50 K to 60 K with a rate of 0.2 K/min (cf. Fig. 5). The shifted Fermi edge of Au clusters on xenon decreases constantly until it vanishes completely. At the same time the Fermi edge of the Pb substrate and of clusters coupled to the substrate arises at the reference Fermi energy of 0 eV.

Next we tried to confirm the explanation of the shifts due to the work function differences by investigating the inverse asymmetric system Pb on 60 ML Xe on Au(111). Here, one expects a large positive shift ΔE because of $\Phi_{Pb} < \Phi_{Au}$. Indeed, Fig. 6 shows the expected positive shift to higher energies of about $+1$ eV. This is rather unusual for solid state samples, because no signal is expected above the common Fermi energy. Charging effects do not give an explanation, because positive charging due to electron emission would lead to a shift in negative direction. However, we can give an interpretation in terms of decoupled clusters as schematically depicted in Fig. 4. The right hand side shows the Au(111) substrate referenced to the Fermi energy E_F, together with the sample system Pb/Xe/Au. The Pb clusters are decoupled, and are referenced to the vacuum energy $E_{vac(Au)}$ of the Au(111) substrate. The work function difference $\Delta\Phi = \Phi_{Pb} - \Phi_{Au}$ leads to a shift of the lead-cluster Fermi edge to higher energies, because of $\Phi_{Pb} < \Phi_{Au}$. To compare both asymmetric sample systems, Fig. 7 illustrates the observed shifts in one diagram.

The shift predicted by the work function difference has the same absolute value for both of the asymmetric systems discussed above. The different absolute sizes of the Fermi edge shifts for Au/Xe/Pb and Pb/Xe/Au can be explained by an additional effect: the cluster charging energy in the final state of the photoemission process (light grey arrows) [17–19]. In both cases the contribution of this charging energy is negative. However, in the case of Pb/Xe/Au the observed absolute shift is $\Delta\Phi - E_C$ compared to $\Delta\Phi + E_C$ for Au/Xe/Pb.

Because of the broad cluster size distribution the charging energy is not exactly defined, but is given by a correspond-

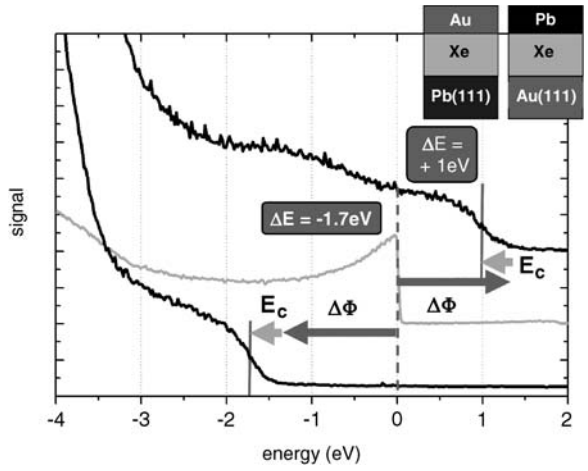

FIGURE 7 Shift of Fermi edge due to work function difference $\Delta\Phi$ (*dark grey arrows*) between Au and Pb. The difference between the shifts for Au/Xe/Pb and Pb/Xe/Au could be explained by the cluster charging energy (*light grey arrows*). Because of a broad cluster size distribution E_C is not exactly defined. A modified interpretation with $\Delta\Phi = 1.1$ eV, as given by the measured work function difference for the two substrates, a smaller charging energy in the case of Pb/Xe/Au and some static charging for the Au/Xe/Pb sample is discussed in the text

ing distribution for E_C. This can also explain the significantly larger width of the Fermi edge for the cluster signal as compared to the sharp Fermi edge for the substrates.

Due to the nanometer size of the clusters a charging energy of the order of 0.1 eV is expected. The measured work functions of the clean Au(111) substrate and the clean Pb(111) substrate as used in Fig. 7 are 5.44 eV and 4.05 eV, respectively. This would correspond to $\Delta\Phi \approx 1.4$ eV.

After adsorption of the Xe film, the work function decreases for both substrates. The shift of -0.32 eV for 1 ML Xe/Au(111) [20] is only slightly smaller than the work function change for the larger film thicknesses up to 160 ML considered here (cf. Fig. 8). This is in agreement with the observation that the work function change saturates after a few monolayers [21]. The work function difference is only slightly changed after Xe adsorption

$$\Delta\Phi = \Phi_{\mathrm{Xe/Au}} - \Phi_{\mathrm{Xe/Pb}} \approx 5.0\,\mathrm{eV} - 3.9\,\mathrm{eV} \approx 1.1\,\mathrm{eV}\,. \qquad (2)$$

This is smaller than the size of the $\Delta\Phi$ arrows in Fig. 7. With $\Delta\Phi = 1.1$ eV one would need only a small charging energy for the lead clusters, but an unrealistically large $E_C \approx 0.6$ eV for the gold clusters. However for the gold clusters some static charging cannot be excluded, as it will be discussed below. In case of the symmetric sample systems Pb/Xe/Pb and Au/Xe/Au, we expect no large work function difference

$$\Delta\Phi = \Phi_{\mathrm{clusters}} - \Phi_{\mathrm{substrate}} \approx 0\,. \qquad (3)$$

It is not a priory clear if Φ for the substrate and/or the clusters should be taken with or without the Xe induced decrease. In addition the cluster work function may be identified with bulk surfaces of different crystalline orientations. This leads to some uncertainty or distribution of $\Delta\Phi$ in the order of 0.3 eV. Similar variations also occured for $\Phi_{\mathrm{substrate}}$ in different experimental runs, e.g. with different preparation procedures, however, this did not change significantly the cluster-induced shifts. As shown in Fig. 9 (top) no large shift of the Fermi edge of the Pb clusters is detected for the system Pb/Xe/Pb. The

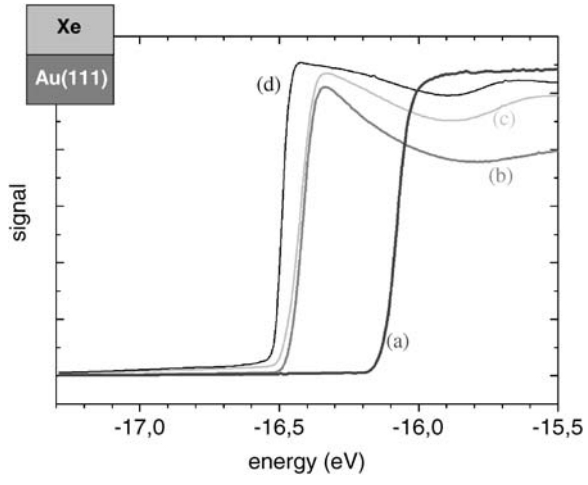

FIGURE 8 Lower cut-off energy of the UPS spectra: (a) pristine Au(111) substrate, (b) 10 ML Xe/Au(111), (c) 30 ML Xe/Au(111) and (d) 160 ML Xe/Au(111). The spectra are scaled to similar maximum signal for better visualization. A bias voltage of -5 eV was applied to the sample. The energy scale is given by the Fermi energy $E_F = 0$ eV

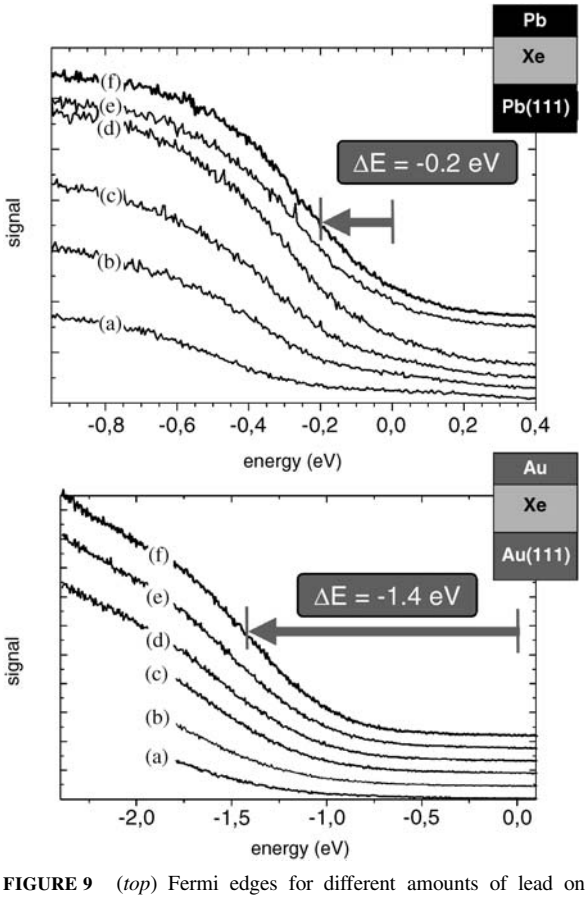

FIGURE 9 (*top*) Fermi edges for different amounts of lead on 60 ML xenon/Pb(111). The small shift can be explained due to the cluster charging energy E_C because of $\Delta\Phi \approx 0$. (*bottom*) Fermi edges for different amounts of gold on 60 ML xenon/Au(111): (a) 0.7 ML, (b) 1.0 ML, (c) 1.4 ML, (d) 1.7 ML (e) 2.1 ML and (f) 2.4 ML. The large shift is at least partly explained due to static charging (for details see text)

small negative shift of about -0.2 eV might be explainable due to the charging energy E_C. But there is some signal also above $E_F = 0$ eV which cannot be explained by E_C but may be due to contributions with $\Delta\Phi < 0$.

The behavior of the other symmetric sample system Au/Xe/Au is different. The UPS results (cf. Fig. 9 bottom) show a large Fermi edge shift of 1.4 eV though there should be no significant work function difference between cluster material and the substrate. To check if there might be a static charging of the sample in this experimental run, we investigated first 120 ML Xe/Au(111). In the UPS spectra we did not observe a shift of the Xe $5p_{1/2}$ peak and take this as an indication that no static charging of the clean Xe film occurs up to this thickness as mentioned above.

However, a significant shift of the $5p_{1/2}$ peak was observed when Au was evaporated on this surface. The shift became already visible at a Au coverage of 0.3 ML – with about 0.5 eV – and increased with the gold coverage. Covering the sample with additional layers of Xe after the Au deposition results in even larger shifts that can amount to several eV. We observed in this case some variation with time and the intensity of the UV light, which is typical for static sample charging.

We can explain these results by assuming the Xe film to have some residual conductivity preventing the growth of static charges, even for large film thicknesses. Partially, at least, it may be due to photoconductivity induced by the He-discharge lamp [22]. In contrast we observed strong static charging in case of a bare Ar film with a thickness of 60 ML which started at film thicknesses above 10 ML. This is possibly connected to the larger gap for Ar (14.15 eV) as compared to Xe (9.3 eV) [22]. Differences for the charge transport in films of the different rare gases were studied in the past e.g., with photoelectron spectroscopy [23]. However, a gold coverage seems to reduce the conductivity of the Xe film, so that some static charging cannot be excluded in this case. We mention here that, in contrast to the samples with Pb clusters, the above-mentioned shift of the Xe $5p_{1/2}$ peak was also observed for the Au/Xe/Au and Au/Xe/Pb samples with a 60 ML xenon film. So far we have to assume that the large shift with respect to Au/Xe/Pb may partly be due to static charging as well, which hinders a quantitative interpretation of results in view of work function changes and charging energies. Nevertheless, this does not alter our qualitative interpretation that, e.g., the positive shift in case of the Pb/Xe/Au sample is not caused by static charges. We expect a quantitative analysis will be possible for future experiments when we will be able to deposit mass selected clusters where the charging energy is better defined.

4 Summary

We could show that it is possible to produce "free clusters on substrate" by metal island growth on a 60 ML xenon film. The cluster-spectra for these systems are referenced to the vacuum energy of the substrate and not to a common Fermi energy like in the case of stronger cluster-substrate interactions.

Photoelectron spectra of free clusters are also referenced to the vacuum energy. However, in our experiments the vacuum energy is no constant parameter of the apparatus, but determined by the substrate material itself. This results in significant energy shifts if one and the same clusters are grown on different substrate materials below the rare gas layer. If the work function of the cluster material is lower than that of the substrate, we observed the remarkable result of a cluster-photoelectron signal above the Fermi energy as defined by the ground level of the sample holder. We measured no static charging of clean Xe films in the photoemission process for thicknesses up to 120 ML. This is in contrast to Ar films where static charging starts for film thicknesses above 10 ML. However, one also has to take care of static charging in the Xe films, whenever metal islands are grown, because this may reduce the residual conductivity of the film, at least in the case of Au islands. The results of the study presented here will also be of great importance to corresponding experiments performed by the deposition of mass selected clusters, which we will conduct in the future.

ACKNOWLEDGEMENTS This work was supported by the Deutsche Forschungsgemeinschaft (SPP 1153 and GK 726).

REFERENCES

1 K. Fauth, M. Heßler, D. Batchelor, G. Schütz: Surf. Sci. **529**, 397 (2003)
2 T.R. Ohno, J.C. Patrin, U.S. Ayyala, J.H. Weaver: Phys. Rev. B **44**, 1891 (1991)
3 L. Huang, S.J. Chey, J.H. Weaver: Phys. Rev. Lett. **80**, 4095 (1998)
4 H. Haberland, M. Mall, M. Moseler, Y. Qiang, Th. Reiners, Y. Thurner: J. Vac. Sci. Technol. A **12**, 2925 (1994)
5 B. von Issendorff, R.E. Palmer: Review of Scientific Instruments **70**, 4497 (1999)
6 G. Kaindl, T.-C. Chiang, D.E. Eastman, F.J. Himpsel: Phys. Rev. Lett. **45**, 1808 (1980)
7 T. Schmitz-Hübsch, K. Oster, J. Radnik, K. Wandelt: Phys. Rev. Lett. **74**, 2595 (1995)
8 T. Irawan, I. Barke, H. Hövel: Appl. Phys. A **80**, 929 (2005)
9 S. Hüfner: *Photoelectron spectroscopy* (Springer Berlin, Heidelberg, New York, 1995)
10 H. Hövel: Appl. Phys. A **72**, 295 (2001)
11 V.N. Antonov, J.S. Palmer, A.S. Bhatti, J.H. Weaver: Phys. Rev. B **68**, 205 418 (2003)
12 P. Dolle, K. Markert, W. Heichler, N.R. Armstrong, K. Wandelt, K.S. Kim, R.A. Fiato: J. Vac. Sci. Technol. A **4**, 1465 (1986)
13 K. Wandelt: J. Vac. Sci. Technol. A **2**, 802 (1984)
14 S.L. Qiu, X. Pan, M. Strongin, P.H. Citrin: Phys. Rev. B **36**, 1292 (1987)
15 P.H. Citrin, G.K. Wertheim, Y. Baer: Phys. Rev. Lett. **41**, 1425 (1978)
16 B. Richter, H. Kuhlenbeck, H.J. Freund, P.S. Bagus: Phys. Rev. Lett. **93**, 026 805 (2004)
17 G.K. Wertheim, S.B. DiCenzo, S.E. Youngquist: Phys. Rev. Lett. **51**, 2310 (1983)
18 M. Astruc Hoffmann, G. Wrigge, B. v. Issendorff: Phys. Rev. B **66**, 041 404 (2002)
19 H. Hövel, B. Grimm, M. Pollmann, B. Reihl: Phys. Rev. Lett. **81**, 4608 (1998)
20 T. Andreev, I. Barke, H. Hövel: Phys. Rev. B **70**, 205 426 (2004)
21 R.J. Behm, C.R. Brundle, K. Wandelt: J. Chem. Phys. **85**, 1061 (1986)
22 M.L. Klein, J.A. Venables (eds.): *Rare gas solids*, Vol. II (Academic Press, London, New York, San Francisco, 1977)
23 N. Schwentner: Phys. Rev. B **14**, 5490 (1976)